

# Quantum noise spectroscopy of superconducting critical dynamics and vortex fluctuations in a high-temperature cuprate

Zhongyuan Liu,<sup>1,\*</sup> Ruotian Gong,<sup>1,\*</sup> Jaewon Kim,<sup>2,\*</sup> Oriana K. Diessel,<sup>3,4,\*</sup> Qiaozhi Xu,<sup>1</sup> Zack Rehfuss,<sup>1</sup> Xinyi Du,<sup>1</sup> Guanghui He,<sup>1</sup> Abhishek Singh,<sup>5</sup> Yun Suk Eo,<sup>5</sup> Erik A. Henriksen,<sup>1,6</sup> G. D. Gu,<sup>7</sup> Norman Y. Yao,<sup>4</sup> Francisco Machado,<sup>3,4</sup> Sheng Ran,<sup>1,6</sup> Shubhayu Chatterjee,<sup>8,†</sup> Chong Zu<sup>1,6,‡</sup>

<sup>1</sup>Department of Physics, Washington University, St. Louis, Missouri 63130, USA

<sup>2</sup>Department of Physics, University of California, Berkeley, California 94720, USA

<sup>3</sup>ITAMP, Center for Astrophysics, Harvard & Smithsonian, Cambridge, Massachusetts 02138, USA

<sup>4</sup>Department of Physics, Harvard University, Cambridge, Massachusetts 02138, USA

<sup>5</sup>Department of Physics and Astronomy, Texas Tech University, Lubbock, Texas 79409, USA

<sup>6</sup>Institute of Materials Science and Engineering, Washington University, St. Louis, Missouri 63130, USA

<sup>7</sup>Condensed Matter Physics and Materials Science Department,  
Brookhaven National Laboratory, Upton, New York 11973, USA

<sup>8</sup>Department of Physics, Carnegie Mellon University, Pittsburgh, Pennsylvania 15213, USA

\*These authors contribute equally to this work

†To whom correspondence should be addressed; E-mail: shubhayuchatterjee@cmu.edu

‡To whom correspondence should be addressed; E-mail: zu@wustl.edu

(Dated: February 10, 2025)

Characterizing the low-energy dynamics of quantum materials is crucial to our understanding of strongly correlated electronic states. However, extracting universal dynamical features requires resolving correlations at both low energy and momentum. Here, we introduce nitrogen-vacancy (NV) centers in diamond as a novel and powerful quantum sensing platform of superconducting materials. We demonstrate the strengths of our approach by probing several low-energy phenomena in high- $T_c$  cuprate  $\text{Bi}_2\text{Sr}_2\text{CaCu}_2\text{O}_{8+\delta}$  (BSCCO) — gapless quasiparticle excitations, critical fluctuations at the metal-superconductor transition and kinetics of vortices. In the absence of an applied magnetic field, we find a sharp reduction in the NV relaxation time ( $T_1$ ) near the critical temperature  $T_c \approx 90$  K, attributed to supercurrent-fluctuation induced magnetic noise. Crucially, the temperature-scaling of the noise near criticality deviates from the Bardeen–Cooper–Schrieffer (BCS) mean-field prediction and reflects critical order parameter fluctuations, allowing us to determine both static and dynamical critical exponents for the transition. When a small field is applied, we detect a broad and asymmetric reduction of  $T_1$  near  $T_c$ , indicating significant field-induced smearing of the transition. By analyzing the scaling of the BSCCO-induced relaxation rate with the field strength, we unveil evidence in favor of a vortex liquid phase. Finally, deep inside the superconducting phase, we employ NV decoherence ( $T_2$ ) spectroscopy to observe strong magnetic fluctuations in the low-frequency regime, suggesting the presence of complex vortex-solid fluctuations. Our results establish NV-based noise spectroscopy as a versatile platform for probing dynamical phenomena in superconductors, with frequency and length scales complementary to existing techniques.

*Introduction* — Strong electronic interactions are responsible for a plethora of complex emergent phenomena observed in quantum materials. This is perhaps best exemplified by unconventional superconductors, where strong electronic interactions induce a macroscopic quantum coherence of electron-pairs and dissipationless flow of currents [1–3]. Key features of this state are encoded in its low-energy dynamics, manifesting as quasiparticle excitations arising from the breaking of electron pairs [4–6], slow collective modes such as critical pairing fluctuations near the metal–superconductor phase transition [7–11], or topological excitations such as vortices carrying quantized magnetic flux [1, 12–15]. Over the years, several experimental techniques have been developed to probe these universal, low-energy features [16–21]. Broadly, techniques for measuring correlated quantum dynamics may be categorized into scattering methods, local spec-

troscopic probes, and bulk measurements [Fig. 1(a)]. Scattering probes (e.g. X-ray scattering [16]) provide both energy and momentum-resolved data, but they typically require experimental apparatus beyond table-top settings, large sample volumes, and can drive the system out of equilibrium [17, 18]. Local probes such as scanning tunneling microscopy (STM) [19] are applicable to low-dimensional samples and provide lattice-scale spatial resolution, yet they exhibit limited momentum resolution and typically operate at low temperatures. By contrast, bulk measurements (including transport [20] and nuclear magnetic resonance [21]) can operate over a wide temperature range, but generally demand large sample volume. Therefore, resolving spectral features at long wavelengths below the meV scale in two-dimensional materials and thin film samples remains a challenge, leading to an unfulfilled gap for experimental techniques that can

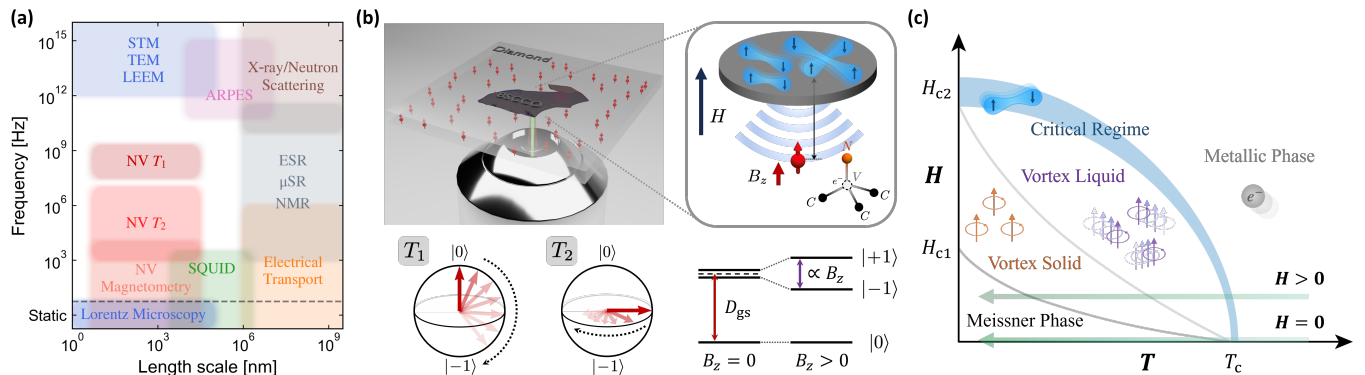


**FIG. 1. NV noise spectroscopy of superconducting dynamics.** (a) Summary of different experimental techniques for probing superconductivity, organized by their frequency and lengthscales, highlighting the complementarity of our qubit-based noise spectroscopy (NV  $T_1$  and  $T_2$ ) and DC magnetometry [22]. Techniques depicted include: electrical transport [20], superconducting quantum interference device (SQUID) [23, 24], Lorentz microscopy [25, 26], X-ray/neutron scattering [16, 27], magnetic resonance with nuclear, electronic, or muonic spins (NMR/ESR/ $\mu$ SR) [21, 28], angle-resolved photoemission spectroscopy (APRES) [29, 30], low-energy and transmission electron microscopy (LEEM/TEM) [31, 32], and scanning tunneling microscope (STM) [19]. Some techniques, while capable of accessing high momentum data, require macroscopic sample volumes and, thus, are only suitable for probing mm-scale samples. Techniques like pump-probe spectroscopy [17, 18], which are known to drive the sample strongly out of equilibrium, are not included. (b) Schematic of the experimental set-up: a thin film ( $\sim 200$  nm thickness) of BSCCO is directly exfoliated onto a diamond plate containing an ensemble of NV centers within a thin layer ( $\sim 50$  nm) beneath its surface. Current fluctuations in the BSCCO sample induce magnetic field noise at the NV locations which can be detected by either depolarization ( $T_1$ ) or decoherence ( $T_2$ ) noise spectroscopy. An out of plane magnetic field  $H$  is applied, which is parallel to the quantization axis of the [111] NV group. The NV exhibits a splitting of its  $|m_s = \pm 1\rangle$  sublevels, which is determined by the local magnetic field  $B_z$ , centered around a zero-field splitting  $D_{gs} = 2.87$  GHz. (c) Schematic H-T phase diagram of a typical type-II superconductor [1–3]. The green arrows indicate zero-field cooling ( $H = 0$ ) and field-cooling ( $H > 0$ ) pathways used in our experiments.

probe equilibrium dynamics at both low-energies and a variety of length-scales.

In this work, we fill this gap by introducing a non-invasive, table-top experimental technique — quantum noise spectroscopy — to probe superconducting dynamics with simultaneous spatial and temporal resolution. Specifically, by using an ensemble of nitrogen-vacancy (NV) centers positioned in close proximity to a thin film high- $T_c$  cuprate —  $\text{Bi}_2\text{Sr}_2\text{CaCu}_2\text{O}_{8+\delta}$  (BSCCO, Bi-2212), we perform noise spectroscopy of superconducting fluctuations as a function of temperature, frequency and applied magnetic field. We demonstrate in-situ detection of spatially resolved dynamics spanning a broad frequency range (MHz to GHz) and length-scales (nm to  $\mu\text{m}$ ), thus offering a powerful complementary toolset to existing techniques for probing superconductivity [Fig. 1(a)].

Our main results are threefold. First, at zero applied field, we study the fluctuations arising from both long-lived quasiparticle excitations at low temperature, and collective critical modes near the metal-superconductor transition temperature  $T_c$ . These fluctuations induce GHz-scale magnetic noise at the location of the nearby NVs which can be characterized via NV depolarization ( $T_1$ ) spectroscopy. Leveraging this capability, we quantitatively measure the characteristic time-scale  $\tau_0$  of critical slowing down of pairing fluctuations near  $T_c$ , as well

as the static and dynamical critical exponents associated with the phase transition [33–35].

Second, we directly probe the broadening of the transition in the presence of a small applied field  $H$ . At non-zero  $H$ , the system hosts superconducting vortices whose dynamics induce additional magnetic field fluctuations. The field dependence of the NV relaxation rate is consistent with the existence of an intermediate-temperature vortex liquid phase [12, 13], where magnetic flux lines diffuse through the superconducting film.

Finally, we employ decoherence ( $T_2$ ) noise spectroscopy to study lower-frequency fluctuations in the MHz regime [36]. Deep within the superconducting phase, we observe a distinct noise mechanism that significantly enhances the NV decoherence rate. These strong, low-frequency magnetic fluctuations potentially arise from thermally assisted flux motion in a vortex solid phase [12, 37, 38].

*Experimental setup*— For our experiments, we choose  $\text{Bi}_2\text{Sr}_2\text{CaCu}_2\text{O}_{8+\delta}$  (Bi-2212), a prominent type-II superconductor with a layered crystal structure and a high critical temperature  $T_c$  exceeding the boiling point of liquid nitrogen [2, 3, 12]. This compound exhibits a rich and complex H-T phase diagram, making it an ideal platform for investigating a variety of different types of low-energy dynamics [Fig. 1(c)]. Bulk crystals of nearly optimally doped BSCCO-2212 are grown by the traveling floating

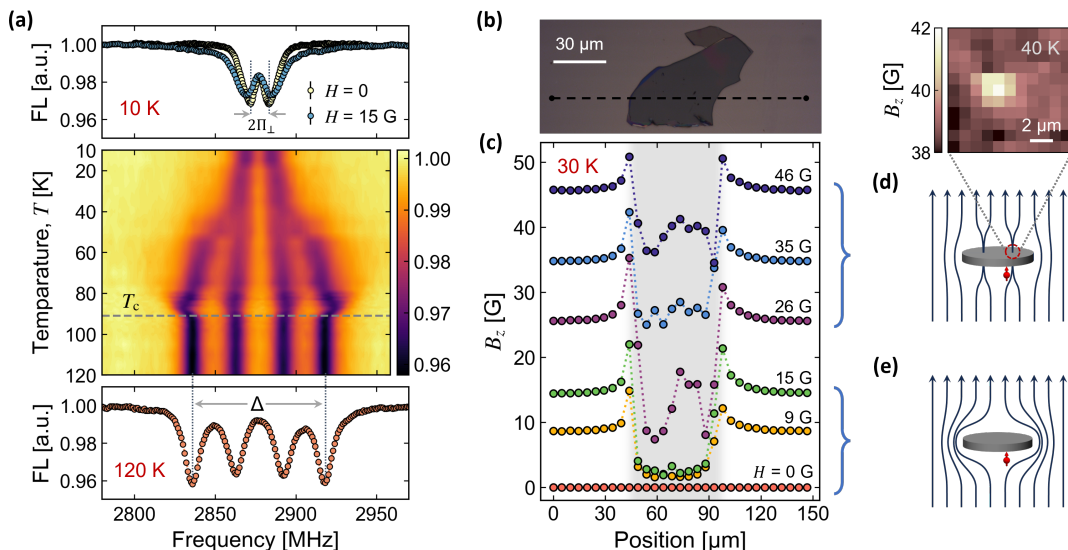


FIG. 2. **Observing Meissner effect and superconducting vortices.** (a) ODMR spectrum of NV centers under BSCCO with an applied field  $H = 15$  G at temperatures from 10 K to 120 K. The colors represent the normalized fluorescence contrast (FL) of the spectrum. The gray dashed line marks the superconducting transition temperature  $T_c \approx 90$  K. Top: at 10 K, ODMR spectrum of NV centers under BSCCO at  $H = 0$  (yellow), where the intrinsic splitting  $2\Pi_{\perp}$  originates from the local electric field [39]. At  $H = 15$  G, the spectrum (blue) remains largely unchanged, indicating a strong magnetic field repulsion due to the Meissner effect. Bottom: when the bias field is not suppressed (120 K), the [111] NV group aligned with the bias field exhibits a splitting  $\Delta$ , while the remaining NVs in other three crystal orientations are degenerate, contributing to the inner two peaks. (b) Optical image of the thin film BSCCO exfoliated on a diamond surface. (c) Local magnetic field  $B_z$  as a function of the applied field  $H$  along a line-cut across the BSCCO [black dashed line in (b)] at 30 K. Compared to NV centers far away from BSCCO, those under BSCCO (gray region) experience smaller local magnetic fields due to the Meissner suppression. Near the edge of the BSCCO,  $B_z$  gets enhanced due to the concentration of the magnetic field lines. (d) Schematic of magnetic flux penetrating a superconductor in its vortex phase. Top: local field image of a defect-trapped superconducting vortex at  $H = 40$  G and  $T = 40$  K. (e) Schematic of magnetic flux being repelled by a superconductor in its Meissner phase.

zone method [40], with  $T_c \approx 90$  K measured via transport (see Methods). To perform noise spectroscopy with NV centers, we exfoliate the BSCCO to a 200 nm thick film and transfer it directly onto a diamond sample containing an ensemble of NV centers in a thin layer  $\sim 50$  nm beneath the diamond surface [Fig. 1(b)].

Each NV center hosts a spin-1 electronic ground state, with Hamiltonian [41]:

$$\mathcal{H} = D_{\text{gs}} S_z^2 + \gamma_e B_z S_z + \Pi_x (S_y^2 - S_x^2) + \Pi_y (S_x S_y + S_y S_x), \quad (1)$$

where  $\{S_x, S_y, S_z\}$  are the spin-1 operators with the N-V axis defining the spin-quantization axis ( $\hat{z}$ ),  $D_{\text{gs}} = 2.87$  GHz is the zero-field splitting between  $|m_s = 0\rangle$  and  $|m_s = \pm 1\rangle$  sublevels,  $\Pi_{\perp} = \sqrt{\Pi_x^2 + \Pi_y^2} = 6.6$  MHz characterizes the coupling to local electric fields [39],  $B_z$  is the local magnetic field along the NV axis, and  $\gamma_e$  is the electronic spin gyromagnetic ratio.

The NV energy levels can be probed via optically detected magnetic resonance (ODMR) spectroscopy where one detects a decrease in NV fluorescence intensity when sweeping the frequency of an applied microwave through the resonances  $|m_s = 0\rangle \leftrightarrow |m_s = \pm 1\rangle$ . In the exper-

iment, we use a [111]-cut diamond crystal and apply a tunable magnetic field  $H$  applied along the out-of-plane direction [Fig. 1(b)]. In this geometry, the NV crystallographic group aligned with the applied field exhibits the largest splitting,  $\Delta = \sqrt{(2\Pi_{\perp})^2 + (2\gamma_e B_z)^2}$  between  $|m_s = \pm 1\rangle$  sublevels, where  $B_z$  includes both contributions from the applied field  $H$  and the  $B_z^s$  generated from the superconducting sample ( $B_z = H + B_z^s$ ). The other three NV groups are always observed to be degenerate.

*Imaging the Meissner effect and flux vortices* — Using the NV centers as sensitive local magnetometers, we begin by determining the presence of superconductivity in BSCCO via the DC Meissner effect [42–47]. After zero-field cooling the sample down to 10 K (well below  $T_c$ ), we perform an ODMR measurement with  $H = 0$  [Fig. 2(a)]. The resulting spectrum shows two resonances separated by the intrinsic splitting  $2\Pi_{\perp}$ . When we then apply a small field  $H = 15$  G, the ODMR spectrum remains largely unchanged, displays only a slightly larger splitting, suggesting that the magnetic field generated by the sample,  $B_z^s \approx -H$ . Indeed, the extracted local field at the NV,  $B_z = 2.5$  G  $\ll H = 15$  G, corroborating the presence of superconducting Meissner phase that expels the external field. We emphasize that the observa-

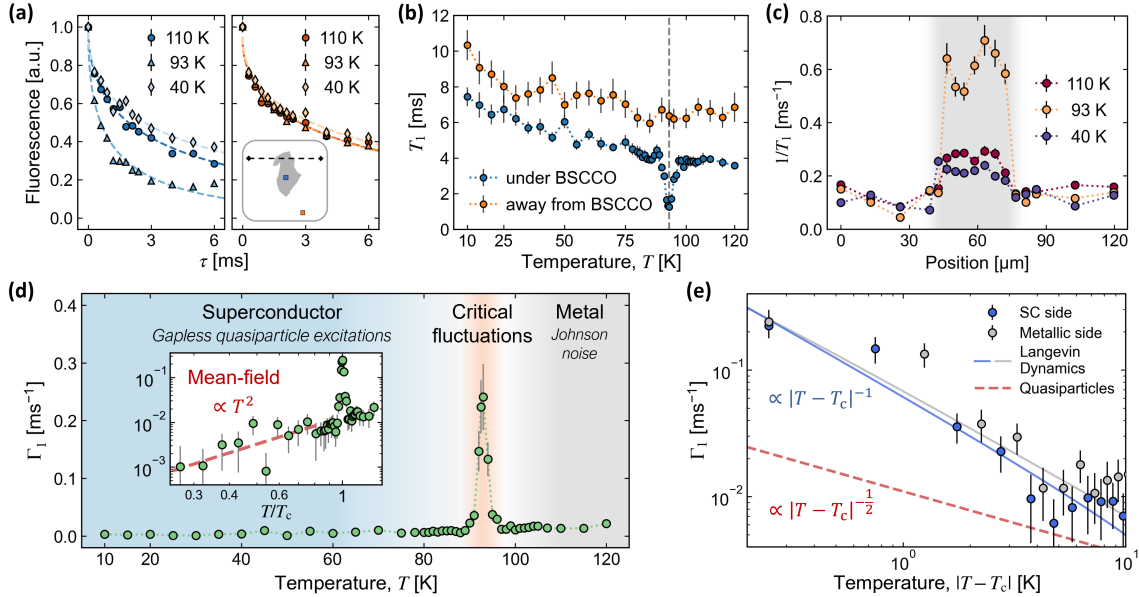


FIG. 3. **Zero-field superconducting fluctuations.** (a)  $T_1$  decay profile for NV centers located under BSCCO (left, blue) and away from BSCCO (right, orange) at 110, 93 and 40 K. Inset: Location of the measured NV centers with respect to the BSCCO sample. (b) The  $T_1$  relaxation timescales as a function of temperature measured on the NV centers located under and away from BSCCO. (c) Spin relaxation rate,  $1/T_1$ , along a spatial line-cut across the BSCCO sample [see (a) inset] at 110, 93 and 40 K. The relaxation rate increases for NV centers under BSCCO (shadow region), particularly near the critical temperature  $T_c$ . (d) The BSCCO-induced decay rate of NVs,  $\Gamma_1(T)$ , as a function of temperature with  $H = 0$ . Inset: a power-law relationship at low temperatures:  $\Gamma_1(T) \propto T^2$ , is consistent with a mean-field approach accounting for nodal quasiparticles in d-wave superconductors. (e)  $\Gamma_1(T)$  as a function of the absolute temperature deviation from the critical temperature,  $|T - T_c|$ , for both the metallic and superconducting (SC) sides of the transition. BCS mean-field quasiparticle dynamics (dashed line) predicts  $\Gamma_1(T) \propto |T - T_c|^{-x}$  with  $x = 1/2$ . However, our experimental data is consistent with  $x \approx 1$ , suggesting that additional superconducting order parameter fluctuations are important. This data aligns closely with a theoretical model of critical Langevin dynamics of the order parameter (solid lines).

tion of a near-complete cancellation of  $H$  underscores the close proximity of our NV sensors to the superconducting BSCCO.

As we increase the temperature, the near-complete expulsion of the external field persists  $T \sim 40$  K. Beyond this point, ODMR spectrum splits into a characteristic four resonances, indicating that the field is no longer fully canceled and that the system has transitioned into a vortex phase, allowing magnetic flux to penetrate the sample. As the temperature further rises, the vortex density increases, raising the local field,  $B_z$  until it reaches the applied field  $H$  at  $T = T_c \approx 90$  K. Interestingly, right below  $T_c$ , the local field  $B_z$  is measured to be slightly greater than  $H$ , which may be attributed to a paramagnetic Meissner effect [48].

Leveraging the local nature of our sensor, we then investigate the spatial dependence of the Meissner suppression. Performing ODMR spectroscopy along a line-cut across the BSCCO [black dashed line in Fig. 2(b)], we directly extract the local magnetic field  $B_z$  as a function of spatial position at  $T = 30$  K [Fig. 2(c)]. Beneath the sample, the Meissner suppression is clearly observed at small applied field  $H \lesssim 20$  G. However, when  $H$  exceeds

25 G, which is on the same order as the independently characterized lower critical field  $H_{c1}$  (see Methods), the Meissner effect is suppressed, and  $H$  is only partially expelled. Crucially, the residual field also exhibits spatial variations across the sample, indicating that magnetic flux penetrates the BSCCO, forming superconducting vortices. One such vortex, possibly pinned by a local defect, is imaged in Figure 2(d), where the locally measured magnetic field  $B_z$  exceeds the applied field  $H = 40$  G due to the bunching of magnetic field lines.

*Zero-field superconducting fluctuations* — Employing the full capabilities of the NV center, we go beyond conventional static magnetic field measurements by performing  $T_1$  relaxometry of the NV to study superconducting fluctuations [Fig. 1(a)]. To this end, we first optically polarize the NV spin state to  $|m_s = 0\rangle$  and subsequently measure the timescale  $T_1$  over which the spin relaxes back to thermal equilibrium [Fig. 3(a)]. Although the intrinsic relaxation of NV centers is primarily driven by spin-phonon interactions within the diamond itself, additional magnetic fluctuations from BSCCO, resonant with the NV's bare frequency ( $D_{\text{gs}} = 2.87$  GHz), can expedite the spin relaxation process and reduce the  $T_1$  of NV.

This is indeed borne out by our data. As shown in Figures 3(a)(b), NV centers located beneath the BSCCO exhibit shorter  $T_1$  compared to NV centers situated away from the BSCCO across the entire temperature range covering the superconducting phase, criticality and metallic phase. This trend is further highlighted in Figure 3(c), which shows that the NV relaxation rate ( $1/T_1$ ) as a function of a spatial line-cut across three distinct temperature regimes, with faster relaxation rates observed in all cases for NV centers beneath the BSCCO sample.

To quantitatively analyze the observed magnetic noise, we extract the BSCCO-induced decay rate,  $\Gamma_1(T)$ , by subtracting the intrinsic relaxation rate — measured from NV centers located far from the BSCCO sample — from the total relaxation rate of NV centers situated beneath the BSCCO [Fig. 3(d)]. At high temperatures,  $T > T_c$ ,  $\Gamma_1(T)$  is finite due to Johnson-Nyquist noise in the metallic phase [49–51]. At very low temperatures,  $T \ll T_c$ , the magnetic noise is significantly suppressed in the superconductor. Crucially, the form of this suppression offers insights into the nature of the pairing symmetry. While in conventional s-wave superconductors  $\Gamma_1(T)$  is exponentially suppressed at low temperatures due to a fully gapped Bogoliubov quasiparticle spectrum [4, 5, 52–55], the presence of nodal quasiparticles in d-wave layered superconductors implies a distinct power-law suppression of  $\Gamma_1(T) \propto T^2$  [52, 53]. Indeed, this expectation is consistent with our observations [Fig. 3(d), inset], corroborating the nodal d-wave nature of superconductivity in BSCCO [2].

The most striking feature of Fig. 3(d) is the sharp and symmetric peak in  $\Gamma_1$  near the critical temperatures  $T_c$ . This peak arises from strong fluctuations in the superconducting order parameter, resulting in enhanced current fluctuations that act as source of magnetic noise at the metal-superconductor phase transition. Crucially, this enhancement is observed across the entire BSCCO sample, as emphasized by the spatial line cut near  $T_c$ , Fig. 3(c). Interestingly, near  $T_c$ ,  $\Gamma_1(T)$  begins to show marked deviations from mean-field expectations for d-wave superconductors. In particular, mean-field theory predicts a divergence of  $\Gamma_1(T) \propto |T - T_c|^{-x}$  with  $x = 1/2$  up to logarithmic corrections [53]. In contrast, the experimentally measured  $\Gamma_1$  at criticality is distinctly more singular, with  $x \approx 1$  [Fig. 3(e)]. This deviation arises because BCS theory neglects both amplitude and phase fluctuations of the superconducting order parameter  $\psi$ , which play a significant role near the critical point [9, 56]. These effects are particularly important for thin-film superconductors where fluctuations are expected to be stronger [1]. Consequently, quantitative characterizing the divergent time-scale associated with dissipative dynamics of the superconducting order parameter near  $T_c$  remains an important open question, which we turn to next.

To properly account for low-energy critical fluctuations, we consider the following phenomenological Langevin dynamics of the superconducting order parameter  $\psi(\mathbf{r}, t)$ .

$$\partial_t \psi(\mathbf{r}, t) = -\gamma \frac{\delta F}{\delta \Psi^*(\mathbf{r}, t)} + \eta(\mathbf{r}, t),$$

$$\text{with } F[\psi] = \int d\mathbf{r} \left[ K |\nabla \psi|^2 + r(T) |\psi|^2 + \frac{u}{2} |\psi|^4 \right], \quad (2)$$

where  $F[\psi]$  is the Ginzburg-Landau free energy functional [1, 10, 11, 34],  $\eta$  is local white noise that captures the effect of coarse-graining, and  $\gamma$  sets the rate of relaxation towards equilibrium [35]. Crucially, by setting  $r(T) = a(T - T_c)$  with  $a > 0$ , we can analyze fluctuations of the order parameter about the minima of the free energy:  $\langle \psi \rangle = 0$  for  $T > T_c$  (metallic) and  $\langle \psi \rangle = \psi_0$  for  $T < T_c$  (superconducting). Such fluctuations in turn leads to enhanced current-induced magnetic noise at the NV frequency  $D_{\text{gs}}$ , enhancing the relaxation rate  $\Gamma_1(T)$  near  $T_c$ . This enhancement of the noise spectral weight at low frequency is a consequence of critical slowing down of order parameter fluctuations: for weak-coupling superconductors it is quantified by the diverging timescale  $\tau_{\text{GL}} = 8\hbar/(k_B|T - T_c|)$  [7, 8] near  $T_c$ .

We find that our theoretical model (see Methods) can faithfully reproduce both the magnitude of the magnetic noise, and the divergence of  $\Gamma_1(T)$  near  $T_c$  with the experimentally observed power-law  $x = 1$  on both sides of the transition [Fig. 3(e)]. In addition, by fitting  $\Gamma_1(T)$  with our model, we extract a quantitative time-scale for critical slowing down  $\tau_0^{\text{fitted,M}} \approx 1.2 \tau_{\text{GL}}$  on the metallic side, and  $\tau_0^{\text{fitted,SC}} \approx 0.2 \tau_{\text{GL}}$  on the superconducting side. Remarkably, our results indicate that the decay rates of the order parameter near criticality are comparable to the analytical weak-coupling results  $\tau_0^{\text{wc,M}} = \tau_{\text{GL}}$  [7] on the metallic side and  $\tau_0^{\text{wc,SC}} = 0.5 \tau_{\text{GL}}$  on the superconducting side [8, 57], even though high  $T_c$  cuprates like BSCCO are expected to be strong-coupling superconductors [58].

Further, our modeling of critical noise also allows us to extract the static critical exponent  $\nu$  that determines the divergence of the order parameter correlation length  $\xi(T) \propto |T - T_c|^{-\nu}$ , and the dynamical critical exponent  $z$  that relates the correlation time  $\tau_0$  and correlation length as  $\tau_0(T) \propto \xi^z$ . The close agreement of the experimental observations with Langevin dynamics of  $\psi$  implies that  $\nu = 1/2$ , and  $\tau_0(T) \propto |T - T_c|^{-1} \propto \xi^2$  implies  $z = 2$ , consistent with expectations for a non-conserved order parameter [35].

*In-field criticality and vortex dynamics* — Next we explore how an out-of-plane magnetic field impacts critical fluctuations. Specifically, we apply a small bias magnetic field and perform  $T_1$  noise spectroscopy at two distinct fields,  $H = 40$  G and  $H = 200$  G. Intriguingly, compared with the zero-field  $\Gamma_1$ , two distinct new features emerge [Fig. 4(a)]: (i) The peak in the measured noise,  $\Gamma_1$ , is



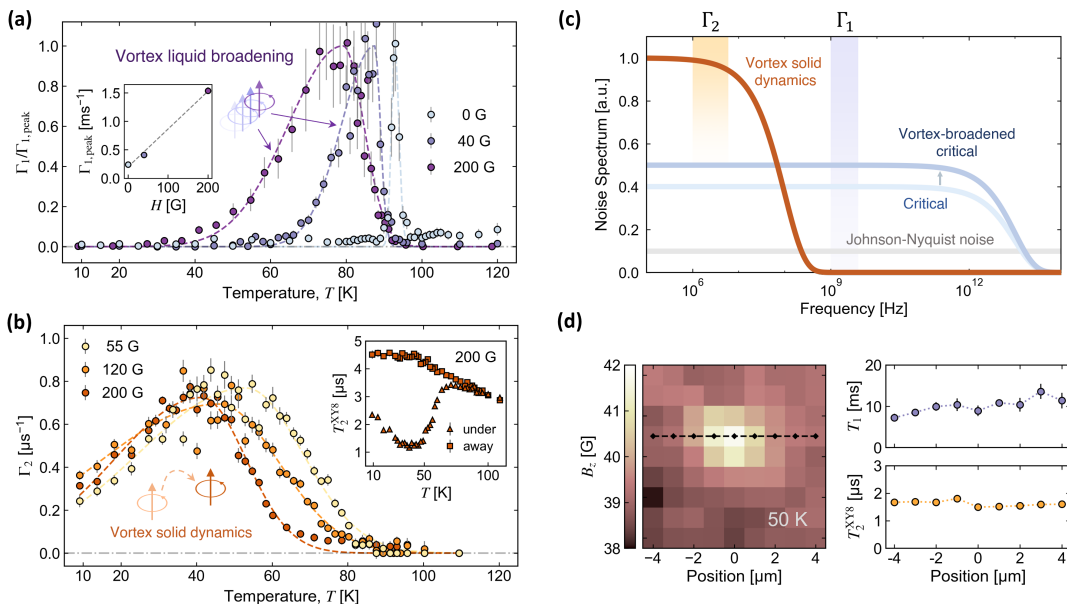


FIG. 4. **In-field criticality and vortex dynamics.** (a) BSCCO-induced relaxation rate,  $\Gamma_1(T)$  (normalized), as a function of temperature at  $H = 0, 40, 200$  G. Inset: the measured peak magnitude of  $\Gamma_1$  as a function of applied field, which is consistent with a linear dependence on the field strength  $H$  (dashed line). (b) BSCCO-induced decoherence rate,  $\Gamma_2(T)$ , as a function of temperature at  $H = 55, 120, 200$  G. Inset: The measured  $T_2^{\text{XY}8}$  decoherence timescale as a function of temperature for NVs under and away from BSCCO at  $H = 200$  G. (c) Schematic of the noise spectrum arising from different dynamical processes in BSCCO. The shaded area marks the most sensitive frequencies of NV relaxation ( $\Gamma_1$ ) spectroscopy and decoherence ( $\Gamma_2$ ) spectroscopy. Since the NV's intrinsic decoherence rate far exceeds its relaxation rate,  $\Gamma_2$  is less sensitive to weak magnetic noise than  $\Gamma_1$ . (d) Left: a trapped vortex imaged in BSCCO under  $H = 40$  G at 50 K. Right: the measured relaxation time  $T_1$  and decoherence time  $T_2^{\text{XY}8}$  of NV centers at different spatial positions across the vortex.

shifted towards a slightly lower temperature. (ii) While the noise signal approaching criticality from the metallic side remains relatively sharp, from the superconducting side, it increases much more gradually and smoothly towards criticality, resulting in a broad and asymmetric spectrum. The former is expected, as a perpendicular field hinders phase coherence and lowers  $T_c$ . The latter can be attributed to a significantly larger fluctuation regime, dominated by the two-dimensional XY critical behavior [13, 14, 59]. Below  $T_c$ , an intermediate vortex liquid phase [12, 15, 38] is expected to form. In this phase, the motion of the superconducting vortices, which trap magnetic flux quanta, can generate strongly fluctuating magnetic fields at the NV, resulting in enhanced noise.

Further evidence for this scenario can be gleaned from the scaling of the peak magnitude of  $\Gamma_1$  with the magnetic field  $H$  [inset, Fig. 4(a)], where the density of vortices  $n_v$  increases with increasing field strength. Within a simple model of diffusive vortex motion (see Methods), the local magnetic noise, measured via  $\Gamma_1(H)$ , scales as  $D_v^{-1}$  where  $D_v \sim v^2 \tau_v$  is the vortex diffusion constant. We expect the vortex scattering time  $\tau_v$  to scale inversely proportional to the vortex density  $n_v$ , and the mean-square speed  $\langle v^2 \rangle$  is primarily determined by thermal energy. Consequently, the measured magnetic noise scales

as  $\Gamma_1(H) \propto n_v \propto H$ , in line with our observation [inset, Fig. 4(a)]. As the temperature decreases further, the vortices either freeze into a lattice or get pinned by defects, resulting in a decrease of  $\Gamma_1(T)$ . This conclusion is consistent with our measurement of noise over a line-cut on a large pinned vortex at low temperatures shown in Fig. 4(d) —  $T_1$  does not change appreciably across the vortex, indicating that pinned vortices do not contribute to magnetic noise in the GHz frequency range.

*T<sub>2</sub> noise spectroscopy of slow vortex dynamics* — At low temperatures, one enters deep into the superconducting phase and the vortex motion freezes out. Nevertheless, with  $H > H_{c1}$ , BSCCO can exhibit complex vortex dynamics, such as thermally assisted flux jumps between different pinning centers, or de-pinning of vortices to exit the superconducting sample, potentially leading to a revival of magnetic noise. However, our data for  $\Gamma_1(T)$  in the low temperature regime exhibits no additional features at finite  $H$ . One possibility is that, unlike the metal-superconducting transition, fluctuations arising from vortex dynamics at low temperatures occur at a much lower frequency range, and therefore eludes detection by  $T_1$  spectroscopy that is only sensitive to the noise spectrum in the GHz range.

To this end, we perform NV decoherence ( $T_2$ ) noise spectroscopy to capture the magnetic noise spectrum in

the MHz frequency range [36, 60–62]. Specifically, after preparing the NV center into a quantum superposition state,  $(|m_s = 0\rangle + |m_s = -1\rangle)/\sqrt{2}$ , we apply an advanced dynamical decoupling sequence (XY-8, see Supplementary Information) to measure the decoherence rate induced by BSCCO,  $\Gamma_2(T)$ , as a function of both temperature and bias external field  $H$  [Fig. 4(b)]. Remarkably,  $\Gamma_2(T)$  exhibits a broad noise spectrum with several prominent features. (i) The onset temperature for  $\Gamma_2(T)$  progressively decreases with increasing field  $H$ , and does not coincide with the peak of  $\Gamma_1$  near criticality. (ii) For a fixed  $H$ ,  $\Gamma_2(T)$  reaches its maximum value at a much lower temperature  $T^*$  than  $\Gamma_1(T)$ ; however,  $H$  is larger than the independently measured  $H_{c1}$  of the sample at  $T^*$  (see Methods), indicating that vortices are still present in the sample. (iii) The maximum value of  $\Gamma_2(T)$  is nearly independent of the external field  $H$ .

To understand this behavior, we begin by noting that the decoherence time  $T_2$  on and off BSCCO is nearly identical in both the metallic phase and near criticality [inset of Fig. 4(b)]. This observation indicates that  $T_2$  noise spectroscopy is less sensitive than  $T_1$  in detecting both Johnson-Nyquist noise and critical current fluctuations. This difference in sensitivity can be attributed to the intrinsic timescale gap between  $T_1$  and  $T_2$ . Specifically, the NV  $T_1$  is around three orders of magnitude larger than  $T_2$ , offering a much longer time window to accumulate the noise signals (see Methods). Consequently, a significantly stronger noise amplitude from BSCCO is required to induce a measurable  $T_2$  in NV sensors.

Furthermore,  $T_2$  measured across a line-cut intersecting a pinned vortex show no position dependence, indicating that frozen vortices also do not contribute to magnetic noise in the MHz frequency range. Combining these observations, we deduce that  $T_2$  is most sensitive to vortex motion within the vortex solid phase [37, 38]. The substantial noise magnitude suggests that it likely originates from thermal fluctuations, which can cause positional jumps of fluxes or flux bundles between different pinning centers, resulting in sudden large changes in the local magnetic field. These dynamics are relatively slow, extending only up to the MHz range. Thus, they are not reflected in  $\Gamma_1$ , but can be directly captured by  $\Gamma_2$  [Fig. 4(c)]. Only at very low temperatures, approximately corresponding to the Meissner phase, does such flux motion begin to freeze out, leading to a decrease in  $\Gamma_2(T)$  below 40 K.

*Summary and Outlook* — For the first time, we demonstrated the use of NV centers as nano-scale quantum sensors to probe three distinct aspects of low-energy dynamics in high- $T_c$  superconductors: gapless quasiparticle excitations at low temperatures, critical superconducting fluctuations near  $T_c$ , and vortex motion in an intermediate temperature range in presence of an external magnetic field. The nanoscale proximity and high sensitivity of our NV sensors, combined with their operational

frequency range spanning three decades (from MHz to GHz) and sub-micron spatial resolution, enable the measurement of local dynamics beyond the capabilities of conventional techniques [Fig. 1(a)].

Looking forward, our work opens the door to several intriguing directions. First, while our current studies involve NV center ensembles with a spread of sensor-sample distances, an immediate future direction is to precisely adjust the distance  $d$  between the quantum sensor and the target material. This can be achieved by using NVs on a scanning tip [63–65], or by creating spin sensors in a given layer of Van der Waals materials such as hexagonal boron nitride [66–69]. By tuning the distance  $d$ , we can adjust the *momentum* filter function to enable controlled probing over a variety of length scales (from nanometers to micrometers) [36], which is crucial for imaging inhomogeneous dynamics in superconductors [45, 70].

Moreover, our measurement of the critical slowing down time-scale  $\tau_0$  places strong constraints on theoretical models of the transition and provides new opportunities to study the mechanisms for order-parameter relaxation near criticality. In fact, a reasonable agreement with the weak coupling result  $\tau_0 = \tau_{GL}$  on the metallic side [7], but a stronger deviation on the superconducting side [8], indicates the necessity for further microscopic investigations of pair dynamics in unconventional superconductors.

Finally, our technique is not limited to BSCCO, and can be readily extended to a variety of superconducting materials. For instance, certain superconductors such as hydrides [71, 72] and nickelates [73, 74] undergo superconducting transitions under high pressure. Thus, moving beyond temperature-driven transitions, the integration of NV centers into high-pressure diamond anvil cells offers a pathway to study how pressure influences critical fluctuations and vortex dynamics [43–45, 51, 70].

*Acknowledgements:* We gratefully acknowledge discussions with Pavel Dolgirev, Chris Laumann, Peng Cai, Panyu Hou, Srinivas Mandyam, and Zhipan Wang. This work is supported by NSF NRT LinQ 2152221, NSF ExpandQISE 2328837, and the Center for Quantum Leaps at Washington University. O. K. D. and F. M. acknowledge support from the NSF through a grant for ITAMP at Harvard University. The work at Brookhaven National Laboratory is supported by the US Department of Energy, office of Basic Energy Sciences, contract No. DOE-sc0012704. E. A. H. and X. D. acknowledge support by the Gordon and Betty Moore Foundation, grant DOI 10.37807/gbmf11560. S. R., Q. X., and Z. R. acknowledge support under National Science Foundation (NSF) Division of Materials Research Award DMR-2236528.

- 
- [1] Tinkham, M. *Introduction to Superconductivity* (Dover Publications, 2004), 2 edn. URL <http://www.worldcat.org/isbn/0486435032>.
- [2] Keimer, B., Kivelson, S. A., Norman, M. R., Uchida, S. & Zaanen, J. From quantum matter to high-temperature superconductivity in copper oxides. *Nature* **518**, 179–186 (2015).
- [3] Zhou, X. *et al.* High-temperature superconductivity. *Nature Reviews Physics* **3**, 462–465 (2021).
- [4] Bardeen, J., Cooper, L. N. & Schrieffer, J. R. Microscopic theory of superconductivity. *Physical Review* **106**, 162 (1957).
- [5] Bardeen, J., Cooper, L. N. & Schrieffer, J. R. Theory of superconductivity. *Physical review* **108**, 1175 (1957).
- [6] Bogoljubov, N. N., Tolmachov, V. V. & Širkov, D. A new method in the theory of superconductivity. *Fortschritte der physik* **6**, 605–682 (1958).
- [7] Larkin, A. & Varlamov, A. *Theory of fluctuations in superconductors*, vol. 127 (OUP Oxford, 2005).
- [8] Schmid, A. A time dependent ginzburg-landau equation and its application to the problem of resistivity in the mixed state. *Physik der kondensierten Materie* **5**, 302–317 (1966).
- [9] Maki, K. The critical fluctuation of the order parameter in type-ii superconductors. *Progress of Theoretical Physics* **39**, 897–906 (1968).
- [10] Cyrot, M. Ginzburg-landau theory for superconductors. *Reports on Progress in Physics* **36**, 103 (1973).
- [11] Schuller, I. K. & Gray, K. Time-dependent ginzburg-landau: from single particle to collective behavior. *Journal of superconductivity and novel magnetism* **19**, 401–407 (2006).
- [12] Blatter, G., Feigel'man, M. V., Geshkenbein, V. B., Larkin, A. I. & Vinokur, V. M. Vortices in high-temperature superconductors. *Reviews of modern physics* **66**, 1125 (1994).
- [13] Halperin, B. & Nelson, D. R. Resistive transition in superconducting films. *Journal of low temperature physics* **36**, 599–616 (1979).
- [14] Beasley, M. R., Mooij, J. E. & Orlando, T. P. Possibility of vortex-antivortex pair dissociation in two-dimensional superconductors. *Phys. Rev. Lett.* **42**, 1165–1168 (1979). URL <https://link.aps.org/doi/10.1103/PhysRevLett.42.1165>.
- [15] Nelson, D. R. Vortex entanglement in high- $T_c$  superconductors. *Phys. Rev. Lett.* **60**, 1973–1976 (1988). URL <https://link.aps.org/doi/10.1103/PhysRevLett.60.1973>.
- [16] Comin, R. & Damascelli, A. Resonant x-ray scattering studies of charge order in cuprates. *Annual Review of Condensed Matter Physics* **7**, 369–405 (2016).
- [17] Kaindl, R. *et al.* Ultrafast mid-infrared response of  $\text{YBa}_2\text{Cu}_3\text{O}_{7-\delta}$ . *Science* **287**, 470–473 (2000).
- [18] De La Torre, A. *et al.* Colloquium: Nonthermal pathways to ultrafast control in quantum materials. *Reviews of Modern Physics* **93**, 041002 (2021).
- [19] Parker, C. V. *et al.* Nanoscale proximity effect in the high-temperature superconductor  $\text{Bi}_2\text{Sr}_2\text{CaCu}_2\text{O}_{8+\delta}$  Using a Scanning Tunneling Microscope. *Phys. Rev. Lett.* **104**, 117001 (2010). URL <https://link.aps.org/doi/10.1103/PhysRevLett.104.117001>.
- [20] Essaleh, L. *et al.* Theoretical and experimental study of AC electrical conduction mechanism in the low temperature range of  $p\text{-CuIn}_3\text{Se}_5$ . *Physica E: Low-dimensional Systems and Nanostructures* **99**, 37–42 (2018).
- [21] Hore, P. *Nuclear Magnetic Resonance*. Oxford Chemistry Primers (Oxford University Press, Oxford, New York, 2015), second edition, second edition edn.
- [22] Barry, J. F. *et al.* Sensitivity optimization for NV-diamond magnetometry. *Reviews of Modern Physics* **92**, 015004 (2020).
- [23] Kirtley, J. R. & Jr, J. P. W. SCANNING SQUID MICROCROSCOPY. *Annual Review of Materials Research* **29**, 117–148 (1999).
- [24] Dusad, R. *et al.* Magnetic Monopole Noise. *Nature* **571**, 234–239 (2019). 1901.10044.
- [25] Harada, K. *et al.* Real-time observation of vortex lattices in a superconductor by electron microscopy. *Nature* **360**, 51–53 (1992).
- [26] Silhanek, A. V., Bending, S. & Lee, S. Local Probes of Magnetic Field Distribution. In *Handbook of Superconductivity* (CRC Press, 2021), 2 edn.
- [27] Mühlbauer, S. *et al.* Magnetic small-angle neutron scattering. *Reviews of Modern Physics* **91**, 015004 (2019).
- [28] Hillier, A. D. *et al.* Muon spin spectroscopy. *Nature Reviews Methods Primers* **2**, 1–24 (2022).
- [29] Liu, G. *et al.* Development of a vacuum ultraviolet laser-based angle-resolved photoemission system with a super-high energy resolution better than 1mev. *Review of Scientific Instruments* **79** (2008).
- [30] Kitamura, M. *et al.* Development of a versatile micro-focused angle-resolved photoemission spectroscopy system with kirkpatrick-baez mirror optics. *Review of Scientific Instruments* **93** (2022).
- [31] Altman, M. S. Trends in low energy electron microscopy. *Journal of Physics: Condensed Matter* **22**, 084017 (2010).
- [32] Moradifar, P. *et al.* Accelerating Quantum Materials Development with Advances in Transmission Electron Microscopy. *Chemical Reviews* **123**, 12757–12794 (2023).
- [33] Landau, L. D. & Lifshitz, E. M. *Statistical Physics: Volume 5*, vol. 5 (Elsevier, 2013).
- [34] Landau, L. D., Lifshitz, E. M. & Pitaevskii, L. *Statistical physics: theory of the condensed state*, vol. 9 (Butterworth-Heinemann, 1980).
- [35] Hohenberg, P. C. & Halperin, B. I. Theory of dynamic critical phenomena. *Reviews of Modern Physics* **49**, 435 (1977).
- [36] Machado, F., Demler, E. A., Yao, N. Y. & Chatterjee, S. Quantum noise spectroscopy of dynamical critical phenomena. *Physical Review Letters* **131**, 070801 (2023).
- [37] Fisher, M. P. A. Vortex-glass superconductivity: A possible new phase in bulk high- $t_c$  oxides. *Phys. Rev. Lett.* **62**, 1415–1418 (1989). URL <https://link.aps.org/doi/10.1103/PhysRevLett.62.1415>.
- [38] Fisher, D. S., Fisher, M. P. A. & Huse, D. A. Thermal fluctuations, quenched disorder, phase transitions, and transport in type-ii superconductors. *Phys. Rev. B* **43**, 130–159 (1991). URL <https://link.aps.org/doi/10.1103/PhysRevB.43.130>.
- [39] Mittiga, T. *et al.* Imaging the local charge environment of nitrogen-vacancy centers in diamond. *Physical review letters* **121**, 246402 (2018).
- [40] Wen, J. *et al.* Large bi-2212 single crystal growth by the floating-zone technique. *Journal of Crystal Growth* **310**,



- 1401–1404 (2008).
- [41] Rovny, J. *et al.* Nanoscale diamond quantum sensors for many-body physics. *Nature Reviews Physics* 1–16 (2024).
- [42] Schluskel, Y. *et al.* Wide-field imaging of superconductor vortices with electron spins in diamond. *Physical Review Applied* **10**, 034032 (2018).
- [43] Yip, K. Y. *et al.* Measuring magnetic field texture in correlated electron systems under extreme conditions. *Science* **366**, 1355–1359 (2019).
- [44] Lesik, M. *et al.* Magnetic measurements on micrometer-sized samples under high pressure using designed nv centers. *Science* **366**, 1359–1362 (2019).
- [45] Bhattacharyya, P. *et al.* Imaging the meissner effect in hydride superconductors using quantum sensors. *Nature* **627**, 73 (2024).
- [46] Nusran, N. *et al.* Spatially-resolved study of the meissner effect in superconductors using nv-centers-in-diamond optical magnetometry. *New Journal of Physics* **20**, 043010 (2018).
- [47] Ho, K. O. *et al.* Studying critical parameters of superconductor via diamond quantum sensors. *arXiv preprint arXiv:2407.16848* (2024).
- [48] Geim, A., Dubonos, S., Lok, J., Henini, M. & Maan, J. Paramagnetic meissner effect in small superconductors. *Nature* **396**, 144–146 (1998).
- [49] Kolkowitz, S. *et al.* Probing johnson noise and ballistic transport in normal metals with a single-spin qubit. *Science* **347**, 1129–1132 (2015).
- [50] Agarwal, K. *et al.* Magnetic noise spectroscopy as a probe of local electronic correlations in two-dimensional systems. *Physical Review B* **95**, 155107 (2017).
- [51] Hsieh, S. *et al.* Imaging stress and magnetism at high pressures using a nanoscale quantum sensor. *Science* **366**, 1349–1354 (2019).
- [52] Chatterjee, S. *et al.* Single-spin qubit magnetic spectroscopy of two-dimensional superconductivity. *Physical Review Research* **4**, L012001 (2022).
- [53] Dolgirev, P. E. *et al.* Characterizing two-dimensional superconductivity via nanoscale noise magnetometry with single-spin qubits. *Physical Review B* **105**, 024507 (2022).
- [54] Kelly, S. P. & Tserkovnyak, Y. Superconductivity-enhanced magnetic field noise. *arXiv preprint arXiv:2412.05465* (2024).
- [55] Li, S. *et al.* Observation of on-and off-resonant interaction between a solid-state spin qubit and a superconducting resonator. *arXiv preprint arXiv:2412.18896* (2024).
- [56] Emery, V. & Kivelson, S. Importance of phase fluctuations in superconductors with small superfluid density. *Nature* **374**, 434–437 (1995).
- [57] Kim, J. & Diessel, O. to appear. *arXiv* (2025).
- [58] Lee, P. A., Nagaosa, N. & Wen, X.-G. Doping a mott insulator: Physics of high-temperature superconductivity. *Reviews of modern physics* **78**, 17–85 (2006).
- [59] Curtis, J. B. *et al.* Probing the berezinskii-kosterlitz-thouless vortex unbinding transition in two-dimensional superconductors using local noise magnetometry. *Physical Review B* **110**, 144518 (2024).
- [60] Xue, R. *et al.* Signatures of magnon hydrodynamics in an atomically-thin ferromagnet. *arXiv preprint arXiv:2403.01057* (2024).
- [61] Ziffer, M. E. *et al.* Quantum noise spectroscopy of critical slowing down in an atomically thin magnet. *Under review at Science, preprint arXiv:2407.05614* (2024).
- [62] Li, Y. *et al.* Critical fluctuation and noise spectra in two-dimensional fe<sub>3</sub> gete<sub>2</sub> magnets. *arXiv preprint arXiv:2407.00647* (2024).
- [63] Maletinsky, P. *et al.* A robust scanning diamond sensor for nanoscale imaging with single nitrogen-vacancy centres. *Nature nanotechnology* **7**, 320–324 (2012).
- [64] Degen, C. Scanning magnetic field microscope with a diamond single-spin sensor. *Applied Physics Letters* **92** (2008).
- [65] Pelliccione, M. *et al.* Scanned probe imaging of nanoscale magnetism at cryogenic temperatures with a single-spin quantum sensor. *Nature nanotechnology* **11**, 700–705 (2016).
- [66] Gottscholl, A. *et al.* Initialization and read-out of intrinsic spin defects in a van der waals crystal at room temperature. *Nature materials* **19**, 540–545 (2020).
- [67] Gong, R. *et al.* Coherent dynamics of strongly interacting electronic spin defects in hexagonal boron nitride. *Nature Communications* **14**, 3299 (2023).
- [68] Stern, H. L. *et al.* Room-temperature optically detected magnetic resonance of single defects in hexagonal boron nitride. *Nature Communications* **13**, 618 (2022).
- [69] Gong, R. *et al.* Isotope engineering for spin defects in van der waals materials. *Nature Communications* **15**, 104 (2024).
- [70] Dailedouze, C. *et al.* Imaging the Meissner Effect and Flux Trapping of Superconductors under High Pressure using N-V Centers. *arXiv e-prints arXiv:2501.14504* (2025). 2501.14504.
- [71] Pickard, C. J., Errea, I. & Eremets, M. I. Superconducting hydrides under pressure. *Annual Review of Condensed Matter Physics* **11**, 57–76 (2020).
- [72] Drozdov, A., Eremets, M., Troyan, I., Ksenofontov, V. & Shylin, S. Conventional superconductivity at 203 kelvin at high pressures in the sulfur hydride system. *Nature* **525**, 73 (2015).
- [73] Sun, H. *et al.* Signatures of superconductivity near 80 k in a nickelate under high pressure. *Nature* **621**, 493–498 (2023).
- [74] Wen, J. *et al.* Probing the meissner effect in pressurized bilayer nickelate superconductors using diamond quantum sensors. *arXiv preprint arXiv:2410.10275* (2024).